Rikky Muller, Mohammad Meraj Ghanbari, and Andy Zhou

Miniaturized Wireless Neural Interfaces

A tutorial

DAVID PIECH

From the U.S. president fist-bumping a brain-controlled robotic arm to monkeys playing brain-controlled Pong, the past few years have had a surge of neural interfaces in the news. Neural interfaces, which are used in brain–machine interface (BMI) and neurostimulation technologies, often conjure images of mind-controlled cyborgs and mind uploading. In reality, they offer incredible hope for patients with intractable neurological conditions.

For example, just nine years ago came the first demonstration of a woman with tetraplegia (paralysis from the chest down) controlling a robotic prosthetic arm through electrical signals recorded directly from her brain, specifically, the motor cortex, which controls movement [1]. For 15 years, she had been unable to perform basic daily tasks, such as eating and drinking on her own, but with a BMI, she demonstrated the ability to pick up a cup of coffee and take a sip.

This was an incredible scientific achievement, and it resulted in multiple ongoing clinical trials around the world, yet there remain challenges to

the practical translation of this technology to patients. The device that connects to a patient's brain pierces her cortex, tunnels wires through her skull, and tethers her to a computer [Figure 1(a)]. A smaller, fully implantable, and wireless interface would ease chronic use and significantly reduce the risk of infection. During the past decade, significant advances have been made toward this goal, with numerous opportunities for development ahead.

Neuromodulation technologies are another type of neurotechnology that stimulates the brain, spinal cord, and peripheral nerves to modulate neural

activity and treat the symptoms of advanced neurological disorders. For example, deep brain stimulation devices [Figure 1(a)] provide electrical stimulation to regulate dysfunctional neural circuits, much like a pacemaker for the brain, and are used to treat Parkinson's disease, dystonia, and more [2]. The devices consist of very long electrodes that are implanted in deep brain structures and a pulse generator that is implanted in the chest cavity and transmits waves of voltage or current to targeted brain regions. Similarly, peripheral nerve stimulators are used to regulate physiological functions, from modulating blood pressure [3] to easing inflammation in rheumatoid arthritis [4]. Neural stimulation can also be used to provide sensorimotor feedback to BMIs, enabling tactile and proprioceptive reactions [5]. These technologies significantly impact the quality of life for many patients, but there remain numerous opportunities for improvement in miniaturization, intelligence, and the invasiveness of implantation.

Implantable neural interfaces are medical devices that require U.S. Food

> **Peripheral nerve stimulators are used to regulate physiological functions, from modulating blood pressure to easing inflammation in rheumatoid arthritis.**

and Drug Administration approval, and they are designed by interdisciplinary teams that, importantly, include biologists and clinicians. Patient safety and the invasiveness of implantation are of paramount concern, making implant volume and power dissipation key to designs. Wireless ICs have paved a path toward fully implantable and minimally invasive neural interfacing. The black elements in Figure 1(b) are the components required for a bidirectional (recording and stimulating), wireless neural interface. A power source, typically in the form of a battery, antenna, or energy harvesting element, is used to power the implant. Wireless data transmission eliminates cables, enabling surgeons to close implant incisions, greatly reducing infection risk. Mixed-signal recording circuits amplify and digitize neural

signals from the electrodes, while stimulator circuits and a controller provide the needed voltage or current to excite the neural tissue. In a closed-loop device, integrated edge compute and machine learning [Figure 1(b), in gray] can reduce the wireless burden by enabling devices to make decisions in situ and with low latencies. These building blocks are common across many types of BMIs and neurostimulation implants, and the past decade has included significant advances in the design of all these components.

There are three major trends driving current technological progress in neural interfaces, including the following:
1) sensor–IC integration for scaling the number of electrodes
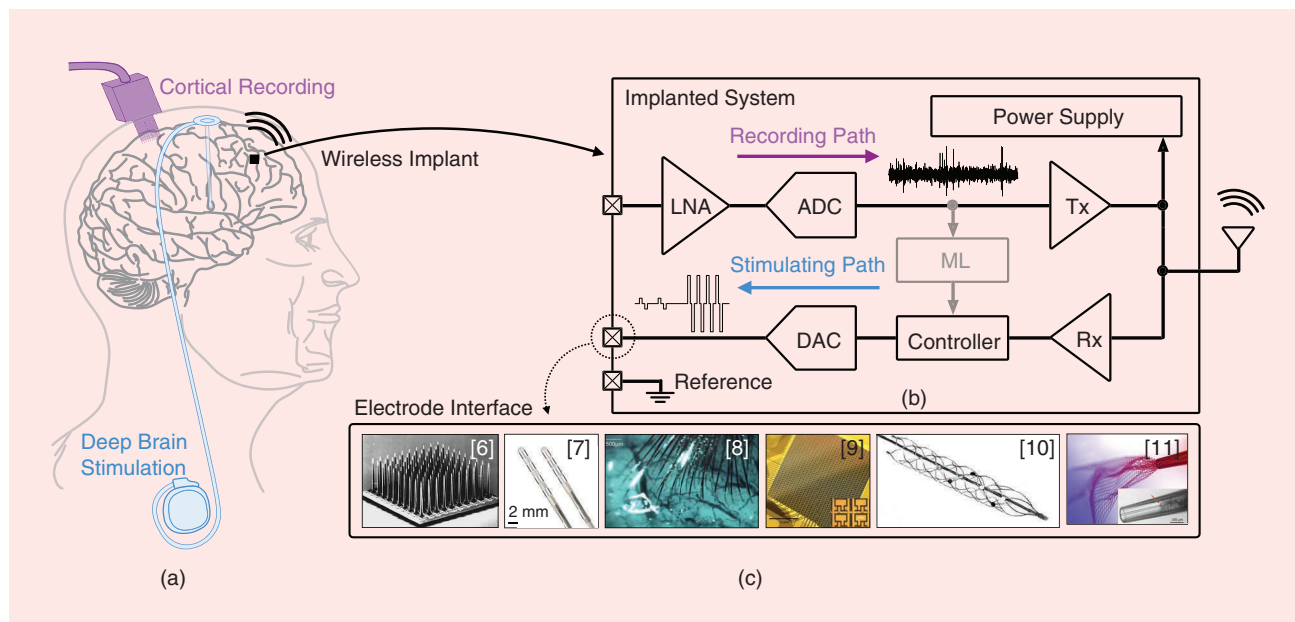2) closing the loop
3) miniaturizing wireless implants.

FIGURE 1: (a) Two clinical neural interfaces: a percutaneous neural recording implant similar to [1], and a deep brain stimulator. (b) Components for an implantable bidirectional (black) or closed-loop (black and gray) wireless neural interface. (c) Example neural interface electrodes. [From left to right (adapted from Utah microelectrode array [6], SENSIGHT by Medtronic [7], ultrathin polymer threads by Neuralink [8], high-density neural matrix [9], Stentrode by Synchron [10] and ultraflexible syringe-injectable mesh [11]).] LNA: low-noise amplifier; ADC: analog-to-digital converter; Tx: transmitter; ML: machine learning; DAC: digital-to-analog converter; Rx: receiver.

> **Patient safety and the invasiveness of implantation are of paramount concern, making implant volume and power dissipation key to designs.**

Scale

The human brain has roughly 86 billion neurons. How many we need to record from remains an open question with an application-dependent answer. Since we are still very much in an era of discovery of how the human brain functions and stores and processes data, the general trend has been to record from as many neurons as possible by scaling the recording devices' channel counts. Sensor–IC integration has been one of the major driving advances in scale. The development of the Utah Array (Figure 1) [6], a microfabricated polysilicon electrode array, enabled neural recording from 100 electrodes at a 400-μm pitch. Designers recognized an opportunity to improve the interface by designing an IC to record from the array and transmit data wirelessly, freeing the subject from cumbersome cabling and instrumentation [14].

The current state of the art has scaled to thousands of channels, with examples provided in Figure 2. Neuralink's 1,024-channel recording and stimulation chip connects to flexible, thread-like electrodes through feedthroughs in a custom hermetic package [8]. IMEC's Neuropixels 2.0 probe [12] integrates 5,120 electrodes directly over circuitry in a long shank structure that is etched directly from a CMOS substrate. Paradromics's Argo system [13] has more than 65,000 flexible wire electrodes bonded to a 256 × 256 amplifier array (Figure 2). High channel counts necessitate local data compression [8], wired connections [12], [13], and edge computing to manage data rate demands. The design of recording circuits to manage the power and data demands of scale have been the subject of numerous review articles and tutorials [15]–[17].

Closing the Loop

Closed-loop neural interfaces build on BMI and neuromodulation technologies to measure neural signals, decode the signals through advanced algorithms, and stimulate to affect a therapeutic intervention and provide sensory feedback. As an example, traditional neuromodulation devices run open loop and are programmed by neurologists who tune patient-specific parameters based on heuristic assessments of therapeutic effects [18]. The process can take months and sometimes years. Open-loop devices also stimulate far more than required, draining device batteries and potentially causing unwanted side effects. Closing the loop to auto-mate the optimization of stimulation patterns has the potential to enable faster and better outcomes for patients while reducing costs and improving accessibility [19].

A major area of progress is the development of closed-loop systems on chip that integrate machine learning with stimulation and recording circuits [Figure 1(b)] [20]. Low-power and low-latency classification of neural signals on-chip can enable smart and miniaturized devices, and new techniques are being developed for a multitude of applications to enable online learning and unsupervised approaches for on-chip classification of neural signals [19], [21].

Miniaturization

There has been significant effort to make devices that are extremely miniaturized, flexible, less invasive to implant, and more biocompatible. Histological studies during the past decade have shown that large rigid structures in the brain cause glial cells [22], which perform maintenance functions in the brain, to coat the foreign bodies, form scar tissue, and insulate the electrodes, reducing the amplitude and bandwidth of the neural signal. Current literature suggests that to avoid cell damage entirely, electrodes should be the same order of magnitude as the diameter of a neuron.

The quest for brain-compatible electrodes has created an entire branch of material science dedicated to the fabrication of thin, flexible electrodes, such as ultrathin polymer threads [8] and conformable thin films [9]. Electrodes that do not require surgical implantation, such as syringe-inserted foldable meshes [11] and stents placed through the vasculature [10], also offer significant advantages in invasiveness and patient safety. Of course, to implant an entire device in this minimally invasive manner, the electronics must fit within the dimensions of syringes and stents, requiring the entire chip, power source, assembly, interconnect, and encapsulation to have dimensions on the scale of 2 mm or less.
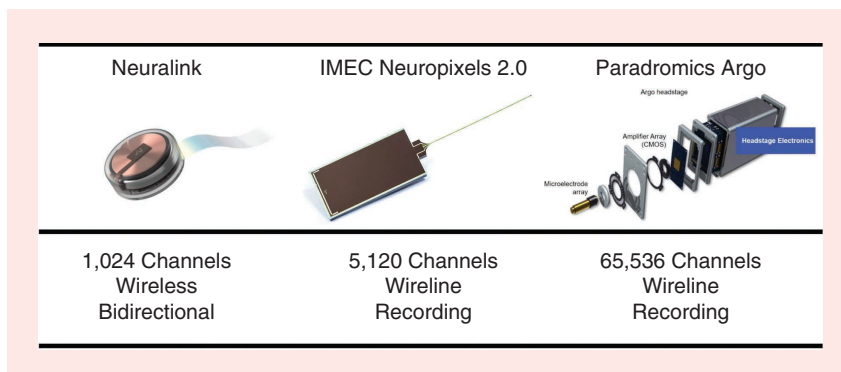

Neuralink	IMEC Neuropixels 2.0	Paradromics Argo
1,024 Channels Wireless Bidirectional	5,120 Channels Wireline Recording	65,536 Channels Wireline Recording

FIGURE 2: Examples of high-channel-count neural interfaces. [From left to right (adapted from Neuralink [8], Neuropixels 2.0 by IMEC [12] and Argo by Paradromics [13]).]
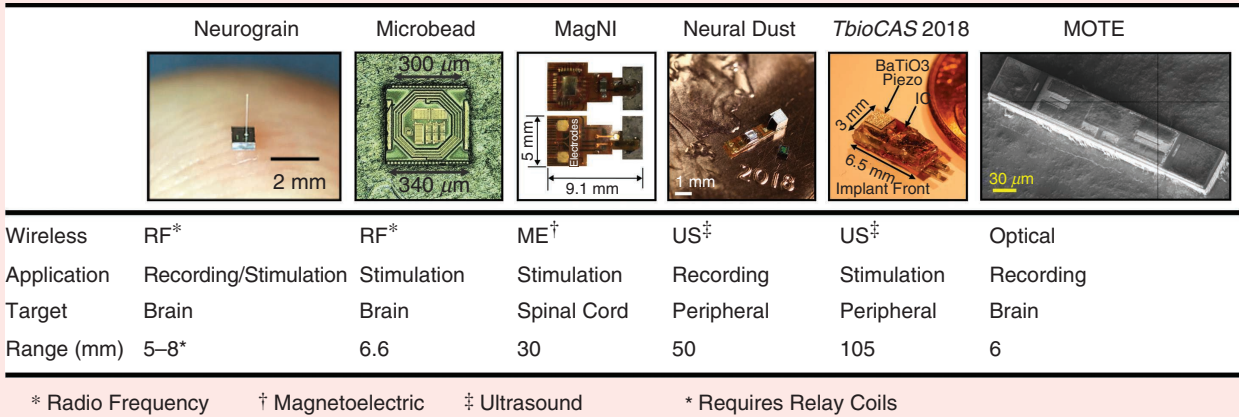
	Neurogram	Microbead	MagNI	Neural Dust	*TbioCAS* 2018	MOTE
Wireless	RF*	RF*	ME†	US‡	US‡	Optical
Application	Recording/Stimulation	Stimulation	Stimulation	Recording	Stimulation	Recording
Target	Brain	Brain	Spinal Cord	Peripheral	Peripheral	Brain
Range (mm)	5–8*	6.6	30	50	105	6

* Radio Frequency   † Magnetoelectric   ‡ Ultrasound   * Requires Relay Coils

FIGURE 3: Examples of recent miniaturized wireless neural implants. [From left to right (adapted from Neurogram [23], Microbead [24], MagNI [25], Neural Dust [26], ultrasonically-powered nerve stimulator implant [27] and MOTE [28]).] MagNI: magnetoelectric neural implant; *TbioCAS*: IEEE Transactions on Biomedical Circuits and Systems; MOTE: microscale opto-electronically transduced electrode.

Recent wireless implants have scaled to the millimeter and even submillimeter scale to record and stimulate brain and peripheral nerve activity. Since batteries do not provide sufficient energy at such scales and periodically need to be surgically replaced, researchers have investigated a multitude of approaches for wirelessly delivering power to and communicating with miniaturized devices (Figure 3). Common wireless powering modalities utilize electromagnetic [23]–[25], acoustic [26], [27] and optical sources [28]. To understand some of the limitations on how small such neural interfaces can get, the remainder of this article consists of a tutorial that focuses on specific design considerations for an ultrasonically powered implantable neurostimulator.

Neurostimulation

To begin to understand how these devices work, we must start at the level of a single neuron (Figure 4). Relative to extracellular fluid, neurons have a negative resting voltage across their membrane. They receive input signals from many neurons that temporarily raise or lower this membrane potential until a threshold is exceeded and causes them to fire an action potential. The action potential propagates down the cell and is part of the signal cascade that is an input to the next cell. It also releases ions into the extracellular fluid that are measurable by nearby electrodes.

Just as neurons communicate with one another through electrical action potentials and the polarization of cell membranes, electrical stimulation is a way to "write in" or communicate with the brain. The cell membrane of a neuron can be modeled as a capacitance, and the application of a charge from an external source can initiate the same processes as other natural inputs. Neurostimulation devices send patterned pulses of current through electrodes that can either excite neurons to fire or inhibit firing. There are other emerging methods to modulate brain activity that may provide more cell-specific activation. These include optogenetics for excitation using light [29], the use of focused ultrasound waves [30], drug delivery directly in the cortex [31], and the use of magnetic fields [32].

Ideally, electrodes make low-impedance contact with tissue, but as our devices get smaller and electrode dimensions shrink, impedances rise and can greatly influence how we design circuits to interface with them. It is therefore extremely important to have a good impedance model of the electrode–tissue interface, which can be modeled with the lumped element circuit model in Figure 5. When the electrode is brought in contact with an ionic solution, charged particles that are dissolved in the liquid are
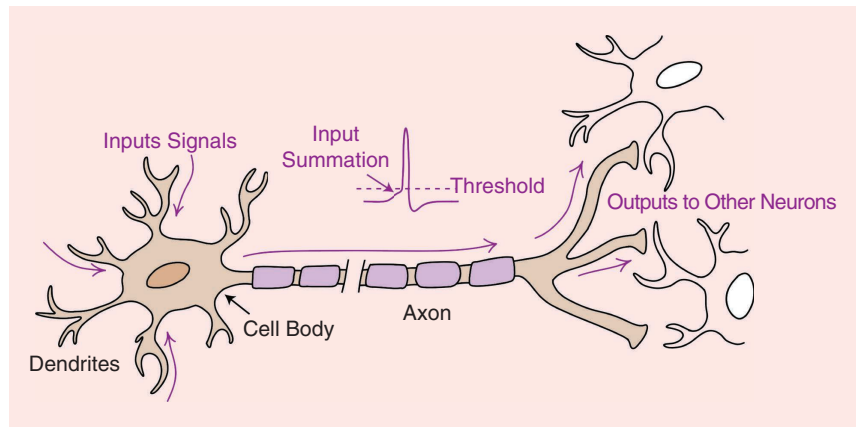

FIGURE 4: An example neuron cell and its action potential, demonstrating the flow of neural information and the origin of electrical neural signals.

attracted to the metal charges and form a double layer. This layer of charged particles, whose average distance from the metal lies on the Helmholtz plane, essentially forms a capacitance (C_{DL}) between the electrode and tissue. Alternatively, a constant phase element, which captures the imperfections of the double layer capacitance, can provide a more accurate model of the impedance.

There is also a parallel charge transfer resistance R_{CT} in the model that accounts for reactions and exchange currents that result at the interface. Both C_{DL} and R_{CT} are electrode material dependent and scale with the effective surface area of the electrode, with the capacitance increasing and the resistance decreasing. Exemplary values for various materials can be found in [33]. The best electrode metals will be inert, low impedance, and biocompatible and have high charge delivery capacity; they include platinum, platinum alloys, and iridium oxide [34].

Here, R_S, which is in series with the other elements, is the resistance of the tissue itself and dependent only on electrode geometric dimensions and the resistivity of the tissue. A round, flat electrode with radius a has a spread resistance of

$$R_S = \frac{\rho}{4a},$$

where ρ is the tissue resistivity. Any interconnect between the stimulator and the electrode may be modeled in series with R_S.

Figure 6 illustrates some common monophasic [Figure 6(a)] and biphasic [Figure 6(b)] stimulation waveforms. While voltages can be used, current provides a more controlled charge delivery since it is agnostic to electrode and tissue impedance fluctuations. Monophasic cathodic pulses are highly efficacious but leave residual charge at the electrode interface, potentially inducing corrosion and neural tissue damage. A passive recharge phase

may be added after each pulse to short the stimulation electrodes and clear built-up charge; however, this can induce large current spikes. Biphasic stimulation, consisting of a cathodic pulse followed by an anodic pulse in the opposite direction, is used to limit the peak reverse current and promote balance in the total amount of charge delivered. The current amplitude, pulsewidth, period, and interphase gap (which improves efficacy) are tuned on a patient-specific basis.

When stimulating nervous tissue, the most important consideration is patient safety. The Shannon criteria [35] constitute an empirical rule for evaluating the possibility of damage to nervous tissue and relate the maximum charge density per phase (Q/A) to the maximum charge per phase (Q) with a dimensionless constant k:
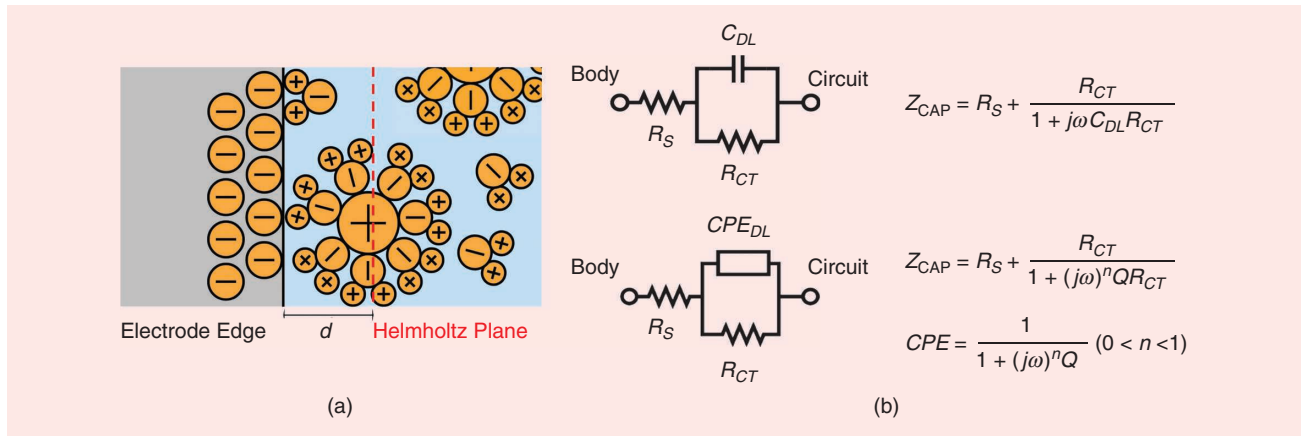
$$\log\left(\frac{Q}{A}\right) = k - \log(Q).$$

FIGURE 5: Circuit models of (a) the electrode–tissue interface using (b) the capacitance (CDL) and a constant phase element (*CPE*DL).
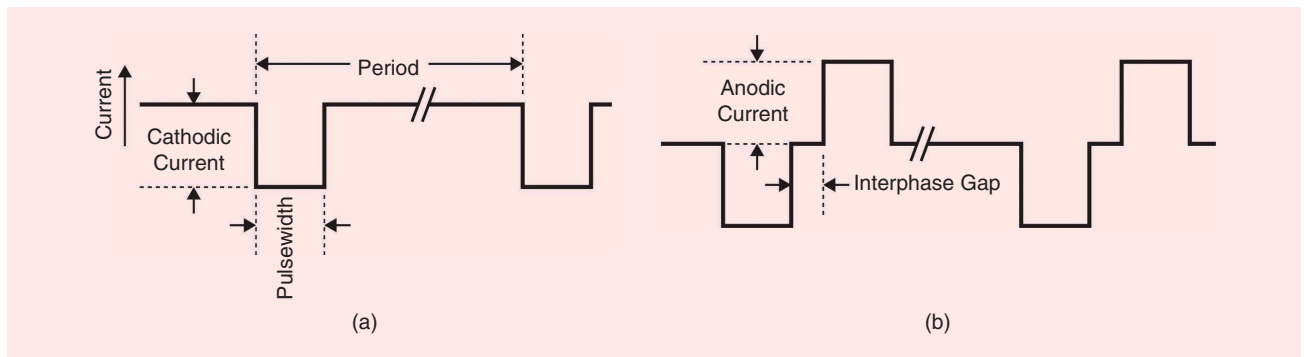

FIGURE 6: (a) A monophasic stimulation pulse train. (b) A biphasic stimulation pulse train with an interphase gap.

Intuitively, both the charge density and charge per phase should play important roles in safety. Charge density captures the notion that passing the same amount of current through a larger-surface-area electrode should be safer and that the total amount of charge that is delivered should also be limited, independent of the electrode size. Shannon observed that experiments where k exceeded 1.85 resulted in tissue damage, leading to the use of this value as an absolute maximum. Clinical deep brain stimulators

observe a maximum charge density of 30 μC/cm^2, a limit derived from a more conservative k value of 1.75. While the Shannon criteria are widely used for stimulation in the central and peripheral nervous systems, a more comprehensive set of safety metrics would capture the effects of frequency, the duty cycle, and the duration of exposure and would be extended to small-area microelectrodes (<30 μm in diameter) [34].

Figure 7(a) reveals the boundary between safe and unsafe stimulation

at $k = 1.85$. The relationship between the charge and charge density at the limit is defined by the electrode area, with an exemplary 1-mm diameter electrode having a limit of less than 1 μC/phase. This safe stimulation boundary can be translated into a relationship between the stimulation current amplitude and pulsewidth, whose product defines the charge in each phase [Figure 7(b)]. Figure 7(c) illustrates one commonly used stimulator topology, the push–pull stimulator, connected to the electrode model. It provides a negative current in one
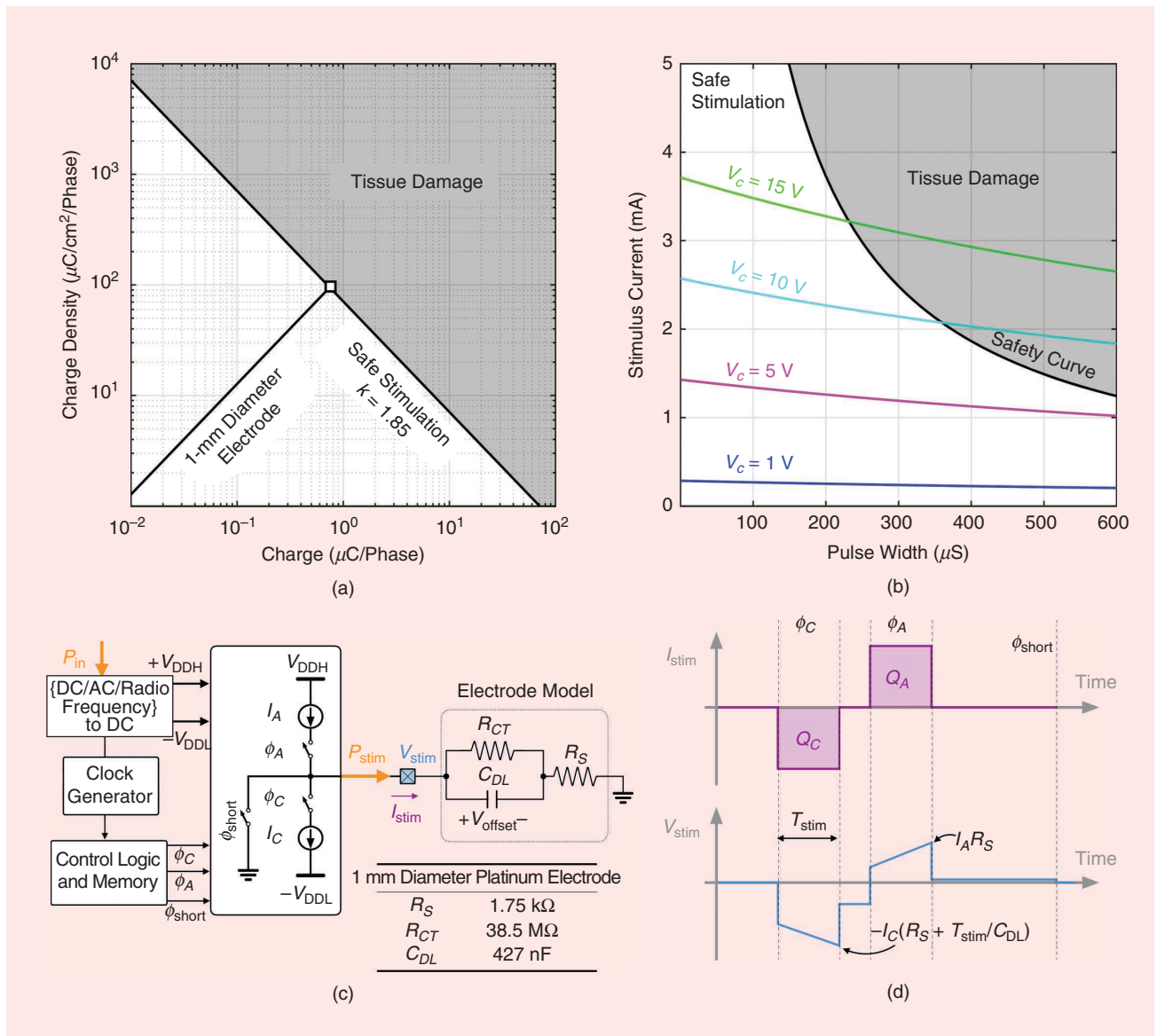

FIGURE 7: (a) A safety curve relating the maximum charge per phase and charge density. (b) Exemplary maximum safe stimulation parameters for a 1-mm diameter platinum electrode. (c) An electrode model connected to push–pull stimulator, with exemplary model values. (d) Waveforms of the stimulation current and voltages for biphasic pulses.

phase with total charge Q_C and a positive current in another phase with total charge Q_A, and it shorts the electrodes in a third phase. For a given stimulation current and duration, the model can be used to calculate the voltage drop measured across the electrode V_{stim}.

The compliance voltage (V_C), or the output voltage range of the stimulator, must be designed to handle these voltage swings, which can be very high and are often the limiting factor for determining the supply voltage [Figure 7(b)]. In the power-constrained environment of an implant, it is important to optimize the overall system efficiency from the power source to the stimulation output power:

$$\eta = \frac{P_{stim}}{P_{in}},$$

where $P_{stim} = 2 \times V_{stim} \times I_{stim} \times T_{stim} \times f_{stim}$. To maximize efficiency, it is advantageous to use the lowest V_{DDH}/V_{DDL} that meets the requirements and can be calculated using the techniques described in this tutorial.

Miniaturizing an Implantable Wireless Neurostimulator

Electromagnetic power coupling is the most common form of wireless power delivery. It is commercially used in devices such as cochlear implants and peripheral nerve stimulators and has been extensively proposed for powering neural implants. In the past few years, ultrasound has emerged as a viable modality for powering and communicating with implants [26], [36]–[38]. An implant utilizes a small ultrasound transducer that converts ultrasound-induced mechanical vibrations to electrical energy. Other forms of wireless energizing include optical and infrared powering [28] and magnetoelectric power transfer [25], [39]. Under the right set of circumstances, all these techniques enable devices to shrink to the millimeter scale. Radio frequency and ultrasound, however, have been demonstrated to provide simultaneous power and bidirectional communication across a single wireless link. This means the number of antennas or transducers on an implant can be reduced to one, resulting in the most volume-efficient designs.

Well-characterized on-chip inductors with moderate quality factors are widely integrated on silicon and greatly simplify the assembly of electromagnetically powered implants [24]. Since the dimensions of on-chip antennas are proportional to the wavelength, implementing millimeter-scale electromagnetic resonators requires operating at a relatively high frequency, e.g., >1 GHz, setting strict limits on the transmitted power and implant depth due to considerable tissue absorption. In contrast, the speed of sound in tissue is almost five orders of magnitude slower than that of electromagnetic waves, and therefore millimeter-scale acoustic resonators can be designed to operate at considerably lower frequencies, e.g., in the megahertz range. Since the acoustic attenuation coefficient is <3 dB/(cm · MHz) for most soft tissues [40], acoustic waves with millimeter-scale wavelengths propagate more efficiently than electromagnetic waves (e.g., up to 9 dB/cm at 1 GHz for muscle [41]). This enables safe power delivery to deep anatomical areas, e.g., most peripheral nerves. While the skull distorts and attenuates the incident ultrasound wave pattern, power can be delivered to implants in the brain through thinned skull [42], [43].

Piezoceramic transducers (piezos) are used to harvest power from ultrasound pressure waves. Since the overall volume of ultrasonic implants is dominated by a piezo, it is helpful to investigate the minimum piezo volume for a given application. We present a design methodology for minimizing the piezo volume [44] that is suitable for deep-tissue neurostimulators that can be used for either peripheral nerve or brain tissue stimulation. The ultrasonic power harvesting system of the stimulator can be modeled by the simplified circuit in Figure 8. The stimulator is represented by an ideal rectifier and a load current sink that requires a minimum voltage headroom of V_L to model the power consumption constraints. The power source is a resonating piezo (actuated by incident ultrasound waves launched by an external transducer) that is modeled by its Thevenin equivalent circuit at resonance. The piezo is actuated by the local acoustic intensity, which is regulated to a maximum of 7,200 W/m² for diagnostic ultrasound [45].

The local ultrasound intensity is a complex function of the operation depth, acoustic properties (the density and speed of sound) of the medium,
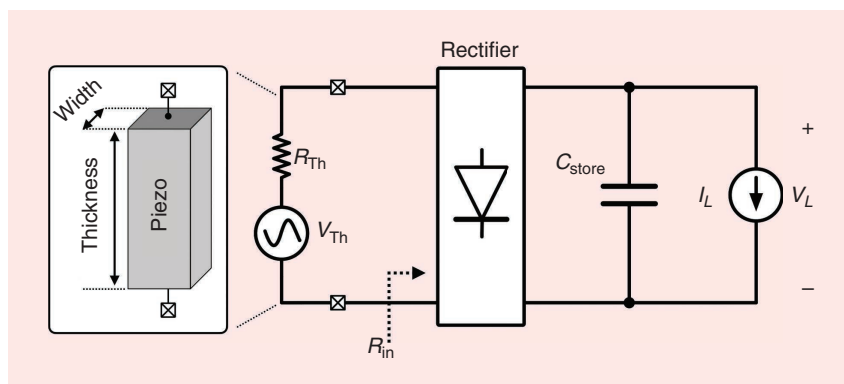
FIGURE 8: The generic ultrasonic implant model.

and type and geometry of the external transducer. We assume that maximum acoustic intensity is locally available at the depth of interest, which is a valid supposition for focused external transducers, e.g., spherical, whose intensity profiles have maxima at their designed focal points. In reality, the intensity in all tissue areas must not exceed 7,200 W/m², and ensuring so requires careful modeling of the external transducer and entire channel, which is beyond the scope of this tutorial.

As shown in Figure 8, the design constraints are V_L and I_L, and the design space is the geometry (the aspect ratio and thickness) of the piezo. For neural stimulation, we target an average current consumption of 100 μA and a minimum rectified voltage V_L of 2.5 V. These numbers

are consistent with those used in previously reported neuromodulating implants in the peripheral nervous system [27], [46] and brain [47] that have been experimentally shown to invoke neural activity in vivo.

The design process begins by characterizing the implant piezo, namely, V_{Th} and R_{Th}, at the resonant frequency. A bulk piezo with a moderate aspect ratio (aspect ratio = width/thickness), used in most ultrasonic implants, mechanically resonates along its major dimension [48]. There are two fundamental resonant frequencies, that is, series and parallel. At either, the reactive components of the piezo electrical impedance cancel out, leaving only a resistance that is modeled by R_{Th}. The piezo model is completed with the open-circuit ac voltage source

V_{Th}. Finite element solvers are used to find the electrical impedance of the piezo, resonance frequencies, R_{Th}, and V_{Th} for various aspect ratios and thicknesses. Solving 3D finite-element models provides a more accurate estimate of these parameters compared to available closed-form 1D analytical expressions, especially for aspect ratios of around one, when there is considerable coupling between different resonant modes that is not easily described with a single set of equations. The simulated parameters are then stored in look-up tables and used throughout the design process. For a lead–zirconate–titanate (PZT-5H) piezo with an aspect ratio of one, these parameters are given in Figure 9(a) and (b). At resonance, V_{Th} linearly scales with the piezo thickness,
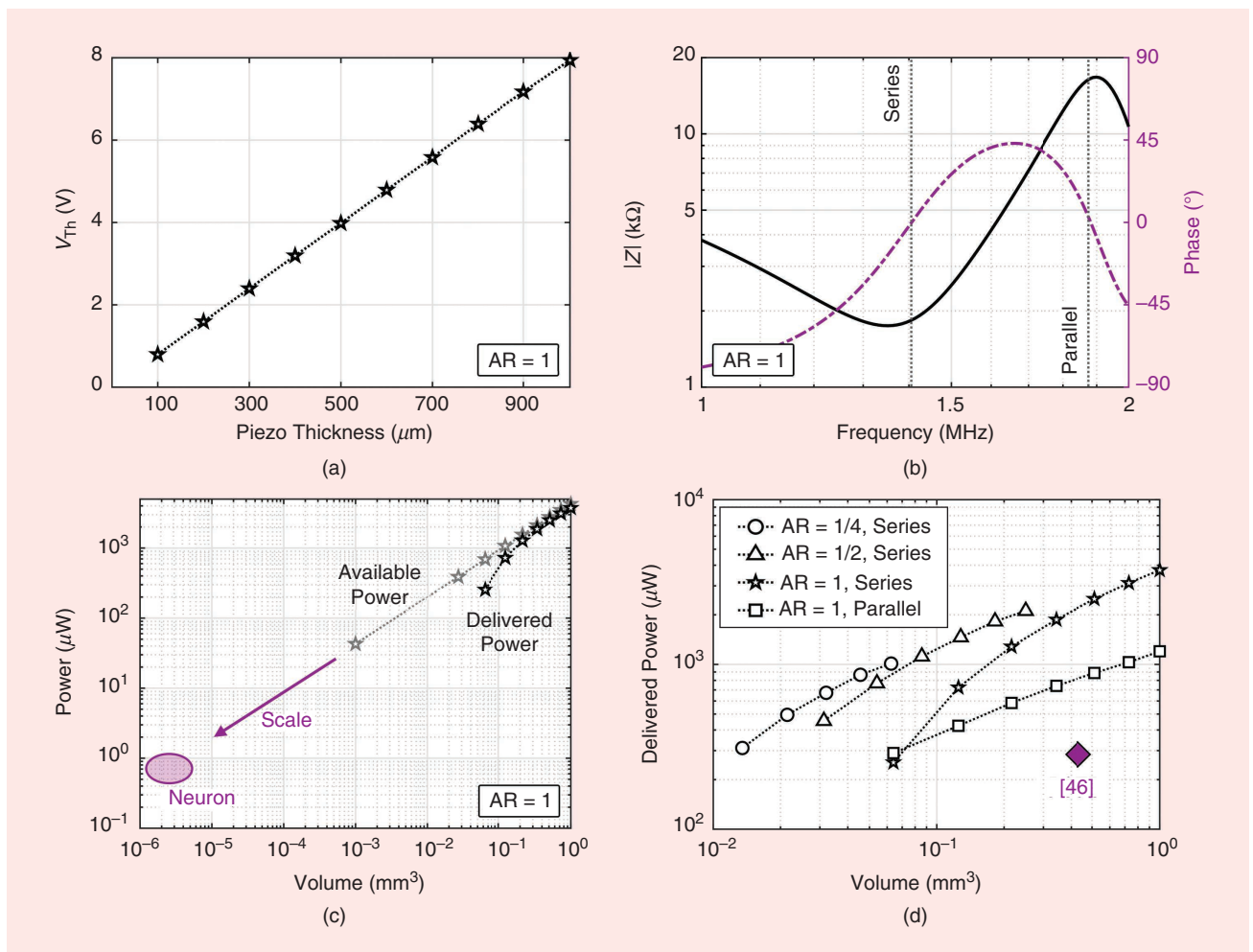

FIGURE 9: The piezo (a) open-circuit voltage, (b) impedance, and (c) calculated maximum available power with the unity aspect ratio (AR) at 7,200 W/m² of local ultrasound intensity. The estimated maximum available power at the neuron dimensions is significant. (d) Designed piezo geometries and a comparison to prior art.

> *From the U.S. president fist-bumping a brain-controlled robotic arm to monkeys playing brain-controlled Pong, the past few years have had a surge of neural interfaces in the news.*

while R_{Th} is independent of thickness and is only a decaying function of the aspect ratio. With a known R_{Th} and V_{Th} for a given geometry (the thickness and aspect ratio), the maximum available power per piezo volume can be calculated. For a PZT-5H piezo with an aspect ratio of one, this is provided in Figure 9(c) at the series resonance frequency.

To harvest the maximum power, the input impedance of the chip R_{in} should be matched to the piezo resistance R_{Th}, and any mismatch will decrease the delivered power. The following equation, derived from the conservation of energy, can be used to approximate the delivered power to the load:

$$I_L \approx \frac{2}{\pi} \frac{V_{Th}}{R_{Th}} \left(1 - \frac{V_L}{V_{Th}}\right)\left(1 - \frac{2}{\pi} a\sin\left(\frac{V_L}{V_{Th}}\right)\right).$$

For a known load voltage, 2.5 V, the preceding expression can be numerically solved for I_L and different combinations of V_{Th} and R_{Th} that are ultimately mapped to different geometries and volumes using the look-up tables. Any geometry that provides $I_L \geq 100 \ \mu A$ is a solution. The same process can be repeated for other aspect ratios at both series and parallel resonant frequencies. A summary of acceptable geometries is in Figure 9(d) for the neural stimulating implant constraints outlined earlier. Interestingly, we find that decreasing the aspect ratio of the piezo roughly maintains the delivered power while decreasing the volume. The smallest piezo volume that delivers 250 μW of power while the rectifier maintains $V_L \geq 2.5$ V is found to be 0.013 mm^3 for a piezo with an aspect ratio of 1/4. This is an order of magnitude smaller than the piezo used in our prior art [46].

In [46], a margin of error was included to account for nonidealities caused by encapsulation, misalignment, and tissue inhomogeneity. Improved encapsulation and tissue modeling and a lower aspect ratio would enable the use of a significantly smaller piezo. Moreover, scaling the piezo size to that of a neuron [Figure 9(c)] could potentially harvest nonnegligible amounts of energy ($\sim 1 \ \mu$W), enough to power a sensor. At these scales, other elements, such as the IC and interconnect, would likely dominate the volume, but this demonstrates that there is significant room for innovation and advancing the state of the art for miniaturizing wireless neural implants.

Summary

This tutorial covered the background of and major trends in neural interface technologies that are used in BMIs and neuromodulation devices. We presented methodologies to ensure safe and efficient neurostimulation and optimize the volume of a wireless ultrasonic neuromodulating implant. So many different parts must come together in the realization of a neural interface that no single tutorial can cover all aspects; in fact, we have only scratched the surface. There are numerous other areas where circuit designers can contribute and significantly advance the state of the art, including machine learning for closing the loop; communication; networking and security for implanted devices; strategies, such as beamforming techniques for coping with misalignment and implant migration; packaging; and more. There are also emerging sensing and stimulation techniques beyond voltage recording and charge-based stimulation and numerous highly impactful evolvin applications that will guide the design of future devices to improve our understanding of the brain, treat neurological conditions, and improve the human condition.

References

[1] L. R. Hochberg et al., "Reach and grasp by people with tetraplegia using a neurally controlled robotic arm," *Nature*, vol. 485, no. 7398, pp. 372–375, May 2012. doi: 10.1038/nature11076.

[2] A. M. Lozano et al., "Deep brain stimulation: Current challenges and future directions," *Nature Rev. Neurol.*, vol. 15, no. 3, pp. 148–160, Mar. 2019. doi: 10.1038/s41582-018-0128-2.

[3] D. T. T. Plachta et al., "Blood pressure control with selective vagal nerve stimulation and minimal side effects," *J. Neural Eng.*, vol. 11, no. 3, p. 036011, June 2014. doi: 10.1088/1741-2560/11/3/036011.

[4] M. C. Genovese et al., "Safety and efficacy of neurostimulation with a miniaturised vagus nerve stimulation device in patients with multidrug-refractory rheumatoid arthritis: A two-stage multicentre, randomised pilot study," *Lancet Rheumatol.*, vol. 2, no. 9, pp. e527–e538, Sept. 2020. doi: 10.1016/S2665-9913(20)30172-7.

[5] M. A. Lebedev and M. A. L. Nicolelis, "Brain–machine interfaces: From basic science to neuroprostheses and neurorehabilitation," *Physiol. Rev.*, vol. 97, no. 2, Apr. 2017. doi: 10.1152/physrev.00027.2016.

[6] C. T. Nordhausen, E. M. Maynard, and R. A. Normann, "Single unit recording capabilities of a 100 microelectrode array," *Brain Res.*, vol. 726, nos. 1–2, pp. 129–140, July 1996. doi: 10.1016/0006-8993(96)00321-6.

[7] "SENSIGHT directional leads," Medtronic, Sept. 1, 2021. Accessed: Aug. 30, 2021. [Online]. Available: https://www.medtronic.com/us-en/healthcare-professionals/products/neurological/deep-brain-stimulation-systems/sensight-lead.html

[8] E. Musk, "An integrated brain-machine interface platform with thousands of channels," *J. Med. Internet Res.*, vol. 21, no. 10, p. e16194, Oct. 2019. doi: 10.2196/16194.

[9] C.-H. Chiang et al., "Development of a neural interface for high-definition, long-term recording in rodents and nonhuman primates," *Sci. Translational Med.*, vol. 12, no. 538, p. eaay4682, Apr. 2020. doi: 10.1126/scitranslmed.aay4682.

[10] T. J. Oxley et al., "Minimally invasive endovascular stent-electrode array for high-fidelity, chronic recordings of cortical neural activity," *Nature Biotechnol.*, vol. 34, no. 3, pp. 320–327, Mar. 2016. doi: 10.1038/nbt.3428.

[11] T. Zhou et al., "Syringe-injectable mesh electronics integrate seamlessly with minimal chronic immune response in the brain," *Proc. Nat. Acad. Sci.*, vol. 114, no. 23, pp. 5894–5899, June 2017. doi: 10.1073/pnas.1705509114.

[12] N. A. Steinmetz et al., "Neuropixels 2.0: A miniaturized high-density probe for stable, long-term brain recordings," *Science*, vol. 372, no. 6539, p. eabf4588, Apr. 2021. doi: 10.1126/science.abf4588.

[13] K. Sahasrabuddhe et al., "The Argo: A high channel count recording system for neural recording in vivo," *J. Neural Eng.*, vol. 18, no. 1, Dec. 2020. doi: 10.1088/1741-2552/abd0ce.

[14] R. R. Harrison et al., "A low-power integrated circuit for a wireless 100-electrode neural recording system," *IEEE J. Solid-State Circuits*, vol. 42, no. 1, pp. 123–133, Jan. 2007. doi: 10.1109/JSSC.2006.886567.

[15] F. Hashemi Noshahr, M. Nabavi, and M. Sawan, "Multi-channel neural recording implants: A review," *Sensors*, vol. 20, no. 3, p. 904, Feb. 2020. doi: 10.3390/s20030904.

[16] X. Liu and J. van der Spiegel, "Neural recording front-end design," in *Brain-Machine Interface*, New York: Springer, 2018, pp. 17–68. doi: 10.1007/978-3-319-67940-2_2.

[17] Y. Liu et al., "Bidirectional bioelectronic interfaces: System design and circuit implications," *IEEE Solid State Circuits Mag.*, vol. 12, no. 2, pp. 30–46, 2020. doi: 10.1109/MSSC.2020.2987506.

[18] T. Koeglsperger, C. Palleis, F. Hell, J. H. Mehrkens, and K. Bötzel, "Deep brain stimulation programming for movement disorders: Current concepts and evidence-based strategies," *Front. Neurol.*, vol. 10, 2019. doi: 10.3389/fneur.2019.00410.

[19] M. Zhang et al., "A one-shot learning, online-tuning, closed-loop epilepsy management SoC with 0.97μJ/classification and 97.8% vector-based sensitivity," in *Proc. Symp. VLSI Circuits*, June 2021, pp. 1–2. doi: 10.23919/VLSICircuits52068.2021.9492429.

[20] G. O'Leary et al., "A neuromorphic multiplier-less bit-serial weight-memory-optimized 1024-tree brain-state classifier and neuromodulation SoC with an 8-channel noise-shaping SAR ADC array," in *Proc. Dig. Technical Papers—IEEE Int. Solid-State Circuits Conf.*, 2020, vol. 2020, Feb. doi: 10.1109/ISSCC19947.2020.9062962.

[21] A. Chua, M. I. Jordan, and R. Muller, "A 1.5nJ/cls Unsupervised Online Learning Classifier for Seizure Detection," in *Proc. Symp. VLSI Circuits*, June 2021, pp. 1–2. doi: 10.23919/VLSICircuits52068.2021.9492392.

[22] A. Ersen, S. Elkabes, D. S. Freedman, and M. Sahin, "Chronic tissue response to untethered microelectrode implants in the rat brain and spinal cord," *J. Neural Eng.*, vol. 12, no. 1, p. 016019, Feb. 2015. doi: 10.1088/1741-2560/12/1/016019.

[23] J. Lee et al., "Wireless ensembles of sub-mm microimplants communicating as a network near 1 GHz in a neural application," *bioRxiv*, Sept. 2020. doi: 10.1101/2020.09.11.293829.

[24] A. Khalifa et al., "The microbead: A 0.009 mm^3 implantable wireless neural stimulator," *IEEE Trans. Biomed. Circuits Syst.*, vol. 13, no. 5, pp. 971–985, Oct. 2019. doi: 10.1109/TBCAS.2019.2939014.

[25] Z. Yu et al., "MagNI: A magnetoelectrically powered and controlled wireless neurostimulating implant," *IEEE Trans. Biomed. Circuits Syst.*, vol. 14, no. 6, pp. 1241–1252, Dec. 2020. doi: 10.1109/TBCAS.2020.3037862.

[26] M. M. Ghanbari et al., "A sub-mm^3 ultrasonic free-floating implant for multi-mote neural recording," *IEEE J. Solid-State Circuits*, vol. 54, no. 11, pp. 3017–3030, Nov. 2019. doi: 10.1109/JSSC.2019.2936303.

[27] J. Charthad et al., "A mm-sized wireless implantable device for electrical stimulation of peripheral nerves," *IEEE Trans. Biomed. Circuits Syst.*, vol. 12, no. 2, pp. 257–270, Apr. 2018. doi: 10.1109/TBCAS.2018.2799623.

[28] S. Lee, A. J. Cortese, A. P. Gandhi, E. R. Agger, P. L. McEuen, and A. C. Molnar, "A 250 μm × 57 μm microscale opto-electronically transduced electrodes (MOTEs) for neural recording," *IEEE Trans. Biomed. Circuits Syst.*, vol. 12, no. 6, 2018. doi: 10.1109/TBCAS.2018.2876069.

[29] V. Emiliani, A. E. Cohen, K. Deisseroth, and M. Häusser, "All-optical interrogation of neural circuits," *J. NeuroSci.*, vol. 35, no. 41, 2015. doi: 10.1523/JNEUROSCI.2916-15.2015.

[30] W. J. Tyler, S. W. Lani, and G. M. Hwang, "Ultrasonic modulation of neural circuit activity," *Curr. Opin. Neurobiol.*, vol. 50, 2018. doi: 10.1016/j.conb.2018.04.011.

[31] C. M. Proctor et al., "Electrophoretic drug delivery for seizure control," *Sci. Advances*, vol. 4, no. 8, 2018. doi: 10.1126/sciadv.aau1291.

[32] M. C. Romero, M. Davare, M. Armendariz, and P. Janssen, "Neural effects of transcranial magnetic stimulation at the single-cell level," *Nature Commun.*, vol. 10, no. 1, 2019. doi: 10.1038/s41467-019-10638-7.

[33] W. Franks, I. Schenker, P. Schmutz, and A. Hierlemann, "Impedance characterization and modeling of electrodes for biomedical applications," *IEEE Trans. Biomed. Eng.*, vol. 52, no. 7, pp. 1295–1302, July 2005. doi: 10.1109/TBME.2005.847523.

[34] S. F. Cogan, "Neural stimulation and recording electrodes," *Annu. Rev. Biomedical Eng.*, vol. 10, no. 1, Aug. 2008. doi: 10.1146/annurev.bioeng.10.061807.160518.

[35] R. v. Shannon, "A model of safe levels for electrical stimulation," *IEEE Trans. Biomed. Eng.*, vol. 39, no. 4, 1992. doi: 10.1109/10.126616.

[36] M. J. Weber, Y. Yoshihara, A. Sawaby, J. Charthad, T. C. Chang, and A. Arbabian, "A miniaturized single-transducer implantable pressure sensor with time-multiplexed ultrasonic data and power links," *IEEE J. Solid-State Circuits*, vol. 53, no. 4, pp. 1089–1101, Apr. 2018. doi: 10.1109/JSSC.2017.2782086.

[37] C. Shi, T. Costa, J. Elloian, Y. Zhang, and K. L. Shepard, "A 0.065-mm^3 monolithically-integrated ultrasonic wireless sensing mote for real-time physiological temperature monitoring," *IEEE Trans. Biomed. Circuits Syst.*, vol. 14, no. 3, pp. 412–424, June 2020. doi: 10.1109/TBCAS.2020.2971066.

[38] S. Sonmezoglu, J. R. Fineman, E. Maltepe, and M. M. Maharbiz, "Monitoring deep-tissue oxygenation with a millimeter-scale ultrasonic implant," *Nat. Biotechnol.*, vol. 39, no. 7, pp. 855–864, July 2021. doi: 10.1038/s41587-021-00866-y.

[39] A. Singer et al., "Magnetoelectric materials for miniature, wireless neural stimulation at therapeutic frequencies," *Neuron*, vol. 107, no. 4, pp. 631–643.e5, Aug. 2020. doi: 10.1016/j.neuron.2020.05.019.

[40] H. Azhari, *Basics of Biomedical Ultrasound for Engineers*. Hoboken, NJ, USA: Wiley, 2010. doi: 10.1002/9780470561478.

[41] D. Laqua, T. Just, and P. Husar, "Measuring the attenuation characteristics of biological tissues enabling for low power in vivo RF transmission," in *Proc. Annu. Int. Conf. IEEE Eng. Med. Biol.*, Aug. 2010, pp. 1437–1440. doi: 10.1109/IEMBS.2010.5626705.

[42] F. J. Fry and J. E. Barger, "Acoustical properties of the human skull," *J. Acoust. Soc. Amer.*, vol. 63, no. 5, pp. 1576–1590, May 1978. doi: 10.1121/1.381852.

[43] P.-C. Tsai, H. S. Gougheri, and M. Kiani, "Skull impact on the ultrasound beam profile of transcranial focused ultrasound stimulation," in *Proc. 1st Annu. Int. Conf. IEEE Eng. Med. Biol. Soc. (EMBC)*, 2009, pp. 5188–5191.

[44] M. M. Ghanbari and R. Muller, "Optimizing Volumetric Efficiency and Backscatter Communication in Biosensing Ultrasonic Implants," *IEEE Trans. Biomed. Circuits Syst.*, vol. 14, no. 6, pp. 1381–1392, Dec. 2020. doi: 10.1109/TBCAS.2020.3033488.

[45] "Marketing clearance of diagnostic ultrasound systems and transducers," U.S. FDA, Rep. no. FDA-2017-D-5372, 2019.

[46] D. K. Piech et al., "A wireless millimetre-scale implantable neural stimulator with ultrasonically powered bidirectional communication," *Nature Biomed. Eng.*, vol. 4, no. 2, pp. 207–222, Feb. 2020. doi: 10.1038/s41551-020-0518-9.

[47] T. L. Skarpaas, B. Jarosiewicz, and M. J. Morrell, "Brain-responsive neurostimulation for epilepsy (RNS® System)," *Epilepsy Res.*, vol. 153, July 2019. doi: 10.1016/j.eplepsyres.2019.02.003.

[48] D. Berlincourt, *Ultrasonic Transducer Materials*. Berlin: Springer-Verlag, 1971.

About the Authors

Rikky Muller (rikky@berkeley.edu) is an assistant professor of electrical engineering and computer science at the University of California, Berkeley, Berkely, California, 94720, USA, where she holds the S. Shankar Sastry Professorship in Emerging Technologies. She is a codirector of the Berkeley Wireless Research Center, a core member of the Center for Neural Engineering and Prostheses, and an investigator at the Chan Zuckerberg Biohub. She received her B.S. and M.S. degrees from the Massachusetts Institute of Technology and her Ph.D. from the University of California, Berkeley. She was the cofounder of Cortera Neurotechnologies and an IC designer at Analog Devices. She is the recipient of numerous fellowships and awards, including the 2021 IEEE Solid-State Circuits Society New Frontier Award.

Mohammad Meraj Ghanbari (ghanbari@berkeley.edu) is pursuing his Ph.D. degree in electrical engineering and computer sciences at the University of California, Berkeley, Berkely, California, 94720, USA. His research interests include analog and mixed-signal ICs, energy harvesting, sensor interfaces, biosensing, and neural recording. He is a Student Member of IEEE.

Andy Zhou (andyz@berkeley.edu) received his B.S. degree in electrical engineering from the California Institute of Technology in 2015. He is a Ph.D. candidate at the University of California, Berkeley, Berkely, California, 94720, USA. His research interests include intelligent neural interfaces and hyperdimensional computing for continuous learning in wearable and implantable devices. He is a recipient of the National Science Foundation Graduate Research Fellowship and a Student Member of IEEE.

SSC